Journal of Biomedical Optics

BiomedicalOptics.SPIEDigitalLibrary.org

Unraveling the molecular nature of melanin changes in metastatic cancer

Kuk-Youn Ju
Simone Degan
Martin C. Fischer
Kevin C. Zhou
Xiaomeng Jia
Jin Yu
Warren S. Warren

SPIE.

Kuk-Youn Ju, Simone Degan, Martin C. Fischer, Kevin C. Zhou, Xiaomeng Jia, Jin Yu, Warren S. Warren, "Unraveling the molecular nature of melanin changes in metastatic cancer," *J. Biomed. Opt.* **24**(5), 051414 (2019), doi: 10.1117/1.JBO.24.5.051414.

Unraveling the molecular nature of melanin changes in metastatic cancer

Kuk-Youn Ju,[a] Simone Degan,[a,b] Martin C. Fischer,[a,c] Kevin C. Zhou,[d] Xiaomeng Jia,[c] Jin Yu,[a] and Warren S. Warren[a,b,c,d,*]
[a]Duke University, Department of Chemistry, Durham, North Carolina, United States
[b]Duke University, Department of Radiology, Durham, North Carolina, United States
[c]Duke University, Department of Physics, Durham, North Carolina, United States
[d]Duke University, Department of Biomedical Engineering, Durham, North Carolina, United States

Abstract. More people die from melanoma after a stage I diagnosis than after a stage IV diagnosis, because the tools available to clinicians do not readily identify which early-stage cancers will be aggressive. Near-infrared pump-probe microscopy detects fundamental differences in melanin structure between benign human moles and melanoma and also correlates with metastatic potential. However, the biological mechanisms of these changes have been difficult to quantify, as many different mechanisms can contribute to the pump-probe signal. We use model systems (sepia, squid, and synthetic eumelanin), cellular uptake studies, and a range of pump and probe wavelengths to demonstrate that the clinically observed effects come from alterations of the aggregated mode from "thick oligomer stacks" to "thin oligomer stacks" (due to changes in monomer composition) and (predominantly) deaggregation of the assembled melanin structure. This provides the opportunity to use pump-probe microscopy for the detection and study of melanin-associated diseases. [DOI: 10.1117/1.JBO.24.5.051414]

Keywords: melanoma; pump-probe microscopy; eumelanin; assembly structure.

Paper 180535SSRR received Oct. 5, 2018; accepted for publication Mar. 11, 2019; published online Apr. 11, 2019.

1 Introduction

In the past several years, advances in nonlinear laser microscopy have provided a new and important approach for diagnosing and grading melanoma by visualizing molecular details of melanin in pigmented skin lesions. This is exceptionally important because of the challenges in detecting aggressive cancers at an early stage.[1,2] The problem is that the standard diagnostic protocol (excision, staining, pathological evaluation) does not identify the most dangerous early lesions. Stage I melanomas make up 78% of all newly diagnosed cutaneous melanomas reported in the U.S. National Cancer Institute SEER database, and of these, 81% are thin lesions (Breslow thickness of $\leq$1.0 mm).[3] For these thin lesions, the standard of care is usually a therapeutic 1-cm margin excision and watchful waiting. But in a study of 1158 patients with thin-lesion melanoma (mean follow-up of 11 years), 5.9% of patients presented with metastatic disease, and 9.4% of patients with no initial evidence of metastases developed recurrences.[4] In fact, whereas only 3% of patients with thin stage I melanomas die of their disease within 10 years, the 1072 such deaths in the SEER-13 registry from 1992 to 2013 represent greater absolute mortality than any other tumor depth of invasive melanoma.[2] So this presents a critical challenge: how do you fix a bad diagnostic gold standard for a bad disease?

Recent work has shown that the femtosecond pump-probe signal of melanin is heterogeneous in skin,[5–8] conjunctival,[9,10] and vulvar[11] tissues, and that this heterogeneity correlates directly with clinical concern. For example, with 720-nm pump and 817-nm probe, the average pump-probe signature changes from negative-dominant, short-lived signals in normal moles to positive-dominant, long-lived signals in metastatic cancer.[5] More recently, a variety of chemical and structural metrics derived from the images were shown to distinguish between primary lesions that went on to cause metastatic cancer and those that did not.[12] So the clinical and diagnostic potential is clear but the molecular basis behind the changes is less obvious. In Ref. 5, the difference between the two signals was noted to agree with differences between eumelanin and pheomelanin, a known difference in bulk composition among benign moles, dysplastic nevi, and melanomas.[13,14] However, imaging of fossilized cuttlefish, where only eumelanin could survive, gave both positive and negative signals.[15] This inspired additional work[7] which showed that many different effects, such as aggregation and iron content, could generate similar changes with eumelanin alone. This did not affect the clinical relevance of the surprising results in Ref. 5 but opened further questions about the molecular basis.

Here we present a comprehensive study starting from model eumelanins, including degradation and cellular uptake, plus comparisons with human tissue. This work provides strong evidence that changes in eumelanin composition, predominantly cellular dissociation of the eumelanin assembly structure, are the fundamental mechanisms behind the observed changes of pigmentation in metastatic melanoma.

Eumelanin, the predominant type of the pigment melanin in nature, plays a dual role in the human epidermal system, both as a well-known protective agent against UV light and free radicals and as a photosensitizer to produce reactive oxygen species (ROS).[16–19] Recent studies have suggested that these conflicting behaviors are related to the unique self-assembled structure of eumelanin. Eumelanin exhibits a characteristic particle nature, where covalently bonded oligomers are stacked and aggregated sequentially to form particles in a scale ranging from tens to

*Address all correspondence to Warren S. Warren, E-mail: warren.warren@duke.edu

hundreds of nanometers.[20] Intact eumelanin particles serve as a protective agent, but eumelanin that has undergone structural dissociation seems to exhibit deleterious behaviors.[21] Dissociation of the self-assembled structure leads to a significant decrease in UV dissipation efficiency.[22] In addition, small fragments generated by oxidative degradation even show higher photochemical reactivity to generate ROS than do intact particles.[22,23] Interestingly, transmission electron microscopy (TEM) has shown that dissociation of the particle structure is more common in melanoma than in benign nevi and normal skin[24,25] but no correlations with metastatic potential have been reported.

The physical properties of eumelanin are also related to the molecular structure of its fundamental monomers. Eumelanin is composed of two major monomeric precursors: 5, 6-dihydroxyindole (DHI) and 5,6-dihydroxyindole-2-carboxylic acid (DHICA). DHI-derived eumelanin oligomers are planar and tend to stack well at the early stage of assembly, whereas stacking between DHICA-derived oligomers is restricted due to their twisted form.[26] Thus, DHI-eumelanin can be considered as an aggregate of "thick oligomer stacks," whereas eumelanin from DHICA-oligomers is an aggregate of "thin oligomer stacks." DHI- and DHICA-derived eumelanin exhibit different optical, magnetic and redox properties,[26–28] reflecting potentially different biological implications. Quantitative measures of DHI and DHICA content in human melanin are complicated by the needed extraction; however, chemical analysis studies suggest a higher level of DHICA-derived eumelanin in human melanoma than in normal melanocytes in skin and hair.[29–31] In addition, dopachrome tautomerase (DCT), a specific enzyme which catalyzes eumelanin biosynthesis to yield DHICA-derived eumelanin, is highly expressed in treatment-resistant, cultured melanoma cells.[32]

This study focuses on determining the relative importance of these bulk chemical changes (eumelanin/pheomelanin ratio, DHI/DHICA ratio, fragmentation) as diagnostic markers for aggressive cancer. We find that the chemical changes of eumelanin observed by near-infrared (near-IR) pump-probe microscopy in pigmented skin lesions are unrelated to pheomelanin content but are related to alterations of the eumelanin self-assembled structure. We image pump-probe differences due to the assembly mode [aggregates of thick (DHI-eumelanin) oligomer stacks and of thin (DHICA-eumelanin) oligomer stacks], and differences due to the degradation from intact particle to deaggregated small fragments. We show that it is fragmentation that distinguishes aggressive (metastatic) cancers from those that are not. By connecting the pump-probe signal of eumelanin to its structure and functions in the melanoma progression, we propose that pump-probe microscopy can not only be a useful diagnostic imaging tool for melanoma but can also be a potent modality to study structure–function relationship of eumelanin in the human pigmentary system.

2 Materials and Methods

2.1 *Preparation of Eumelanin Models*

Squid eumelanin particles were extracted from the ink sacs of *Todarodes pacificus*. After extraction, squid eumelanin particles were purified with sequential centrifugation (20,000 rpm, 10 min) and redispersed in water about 10 times. The morphological shape of squid eumelanin particles was characterized by TEM. Eumelanin from *Sepia officinalis* was provided by Sigma Aldrich.

2.2 *pH-Controlled Disassembly Process*

Eumelanin particle models were disassembled by exposure to deoxygenated alkaline solution, as described previously.[22] The eumelanin (1 mg/mL) suspension and NaOH solution (1N) were purged with N_2 for 20 min to eliminate dissolved oxygen. During purging with N_2, 3.5 mL of NaOH solution was added to the eumelanin suspension (8 mL). After 5 h, 5 mL of deoxygenated KH_2PO_4 solution (1M) was added to the eumelanin suspension for neutralization. The resulting solution was dialyzed using a dialysis kit (Thermo Scientific, Slide-A-Lyzer Dialysis, with molecular weight cutoff of 2000) for 1 day. After dialysis, the subunit fraction entrapped inside the membrane was centrifuged to eliminate residual particles (19,000 rpm, 10 min). After removal of residual particles, subunits were characterized by AFM, photoluminescence spectroscopy, and pump-probe spectroscopy. The subunit fraction [molecular weight (MW) <2000] that passed though the dialysis membrane was collected and concentrated by evaporating the water. The subunit fraction was further dialyzed (Float-A-Lyzer G2 Dialysis Device, with molecular weight cutoff capability of 100 to 500 Da) for elimination of dissolved salts. For AFM analysis, subunits were deposited onto a mica substrate. For deposition of the deaggregated subunits, highly diluted subunit solution was dropped onto the spinning mica substrate (4000 rpm). The height distribution of subunits was then analyzed by AFM (Digital Instruments Dimension 3100 AFM).

2.3 *Preparation of PDCA and PTCA*

Oxidative decomposition of eumelanin in alkaline hydrogen peroxide breaks the two eumelanin monomers (DHI and DHICA) into pyrrole-2,3-dicarboxylic acid (PDCA) and pyrrole-2,3,5-tricarboxylic acid (PTCA), respectively. For the synthesis of PTCA, 100 mg of 5-hydroxyindole-2-carboxylic acid was dissolved in 100 mL of 1 M K_2CO_3 and then oxidized with 4 mL of 30% H_2O_2 by heating under reflux for 20 min. After cooling, 5 mL of 10% Na_2SO_3 was added and the mixture was acidified with 40 mL of 6 M HCl. The acidified solution was extracted twice with 200 mL of ether. The ether extract was washed with 50 mL of water, dried over anhydrous Na_2SO_4, and concentrated to dryness in vacuo. Pale-brown PTCA crystals formed on the walls of the flask and were collected for high-performance liquid chromatography-mass spectrometry (HPLC-MS) analysis. PDCA was synthesized using 5-hydroxyindole in the same manner as previously described for PTCA.

2.4 *Peroxide Oxidation of Melanin Models*

Chemical oxidation of melanin was performed, as described in a previous study,[33] with slight modifications. About 860 μL of 1 M K_2CO_3 and 40 μL of 3% H_2O_2 were added to 100 μL of melanin suspension (1 mg/mL), and the suspension was heated in a boiling water bath for 20 min. After cooling, the residual H_2O_2 was decomposed by adding 20 mL of 10% Na_2SO_3. The mixture was acidified with 500 μL of 6 M HCl. The resulting solution was extracted twice with 7 mL of peroxide-free ether. The ether extract was evaporated to dryness and the residue was dissolved in 200 μL of water. The resulting solution was centrifuged with a centrifugal filter equipped with a semipermeable

membrane (Amicon Ultra centrifugal filter MWCO 3 kDa) and the fraction that passed through the filter was injected into the chromatograph.

2.5 *Cell Culture and Cellular Uptake*

4T1 murine breast cancer cells and macrophage RAW 264.7 cells were purchased from the cell culture facilities at Duke University, North Carolina. The B16 melanoma cell line was provided by the Department of Dermatology at Duke University. 4T1 cells and RAW 264.7 were cultured in RPMI 1640 (Sigma Aldrich, St. Louis, Missouri), containing 10% fetal bovine serum (FBS; Gibco-Thermo, Grand Island, New York), 1% HEPES (Gibco-Thermo, 15630), 1% sodium pyruvate (Gibco-Thermo 11360), and glucose (Sigma Aldrich, G8769). RAW 264.7 and B16 cells were cultured in DMEM high glucose media (Sigma D6429 and Gibco-Thermo 11995-065, respectively) with 10% FBS. 4T1 and RAW culture media received 1% penicillin/streptomycin (Gibco-Thermo 15140-122), whereas antibiotic-antimycotic (Gibco-Thermo 15240-062) was added to the B16 medium. The cell cultures were incubated at 37°C in 5% CO_2 with humidification, and split when 75% confluent into 6-well plates for treatment.

Squid eumelanin particles were added to the cell culture dish at a concentration of 200 μg/mL. After the cells were incubated for 14 h, the dishes were rinsed several times with phosphate-buffered saline (PBS) for removal of the residual particles. After rinsing, the cells were fixed by adding fixative (PBS buffer solution containing 4% formaldehyde and 2% glutaraldehyde). After 2 h, cells were rinsed several times with PBS solution.

2.6 *Preparation of Thin Sliced Cells for TEM*

Fixed cells were stained with OsO_4 by exposure to 1% OsO_4 solution for 1 h. After washing the cells with acetate buffer solution, the cells were further stained with uranyl acetate by exposure to 0.5% uranyl acetate solution for 1 h. By exposure to sequential concentration of ethanol (30%, 50%, 70%, 90%, and 100%) for 10 min, respectively, the cells were dehydrated. The dehydrated cells were exposed to the epoxy resin for 1 day. After replacement with fresh resin, they were placed in an oven and baked (55°C to 60°C) for 2 days. Cells embedded in solidified resin were microtomed and the thinly sliced cells were placed on carbon-coated TEM grids.

2.7 *Pump-Probe Experiment*

Pump-probe signals and images were obtained in a similar manner as previous reports[12] with some modifications. In general, a titanium-sapphire laser was tuned between 770 and 830 nm (80 MHz, Chameleon, Coherent, Inc.) and pumped an optical parametric oscillator (Mira-OPO, Coherent, Inc.) typically tuned between 720 and 730 nm. The pulse cross-correlation, measured by two-photon absorption in Rhodamine-6G, was ~210-fs FWHM. The pump beam was intensity-modulated at 2 MHz with an acousto-optic modulator; the probe beam was unmodulated. Through a mechanical delay stage, the interpulse delay was controlled and the two beams were combined on a dichroic mirror. The two beams were sent to a home-built scanning microscope fitted with an objective (40×, 0.75 NA, Olympus). The power in each beam was adjusted to 0.6 mW impinging on the sample. Multiple repeated pump-probe measurements up to (and including) this power level did not result in appreciable signal changes, thus indicating that the samples were stable at this level of illumination. After transmission through the sample, the beams were collected with a 1.1 NA condenser (Olympus). The pump beam was selectively rejected by a stack of optical filters, and the probe was detected by an amplified photodiode.

Squid eumelanin and subunits samples were homogeneously deposited in agarose gel with a thickness of about 100 μm on a glass substrate. For cell imaging, the pump and probe wavelengths were tuned to 720 and 817 nm, respectively. A dipping objective (40×, 0.75 NA, Olympus) was used for pump-probe imaging of squid eumelanin that were internalized in the cell. Scan speed was 25 ms/line with 512 pixels per line across a 175-μm field of view. Custom MATLAB software was used to process the data files.

2.8 *Phasor Analysis*

Phasor analysis is a simple and powerful tool to differentiate heterogeneous chromophores in pump-probe microscopy.[12] For phasor analysis, a single-frequency sine- (in-phase) and cosine- (out-of-phase) Fourier transform is calculated for a chosen frequency. Because the pump-probe interpulse delays for the datasets are not equidistant, a slightly modified phasor calculation is performed. Instead of a conventional Fourier integration, the integration here is weighted with the inverse of the delay spacing in order to avoid a disproportionately large influence of noise in areas of sparse delay sampling (mostly for very long delays). Phasor coordinates (i.e., the in-phase versus the out-of-phase component) are calculated for each pixel in the image stack and a histogram is constructed. As the pixels in an intensity image can also be color-coded by the phasor coordinates, different components in a pump-probe data stack can be visualized spatially with colorimetric molecular contrast.

2.9 *Biopsy Samples*

As a control eumelanin pigment, a black nevi slide sample from a 30-year-old male and black hair from a 35-year-old male were imaged. Biopsy slides from patients with invasive melanoma were imaged. The biopsy samples were obtained from excised and fixed lesions mounted in paraffin. The patients from whom the biopsy slide samples were taken had undergone sentinel lymph node biopsy (SLNB). All protocols were approved by the Institutional Review Board of Duke University.

2.10 *High-Performance Liquid Chromatography-Mass Spectrometry*

The oxidation products were analyzed by HPLC using an Ultimate 3000 RS system (Thermo Fischer Scientific Inc.) and U-VDSpher PUR C18-E column (1.8 μm, 50 × 2.0 mm, VDS optilab). The mobile phase was 0.1% formic acid in water (solvent A) and 0.1% formic acid in acetonitrile (solvent B). At 1.0 mL/ min, the elution gradient was (min, %B): 0, 0; 1, 0; 12, 25; 14, 25; 16, 0. The UV detector was set at 255 nm absorbance. The standards for peak identification were PTCA and PDCA.

3 Results

3.1 *Characterization of Eumelanin Structure*

We have used two types of natural eumelanin models: cuttlefish (*Sepia officinalis*, hereafter called sepia) and squid (*Todarodes*

pacificus, hereafter called squid). Sepia eumelanin has long been the eumelanin standard because of its high purity and well-characterized self-assembled structure,[20,34] but structural information of squid eumelanin has been sparse. In fact, sepia eumelanin consists of large aggregates of small particles [Fig. 1(b)], with single particle sizes in the aggregate of ~100–150 nm (Fig. S1, in the Supplementary Materials). Sepia eumelanin is readily available from commercial suppliers, but our experience with pump-probe imaging is that although color variations between samples are minor, pump-probe dynamics can be quite variable. On the other hand, pigments extracted from the ink sac of squids are dark brown and consist of single spherical particles with a size range from 50 to 300 nm [Fig. 1(b)]. Elemental analysis (Fig. S2, in the Supplementary Materials) has shown that the pigment from squid ink is indeed eumelanin, as it does not contain any detectable sulfur content (which would indicate the presence of pheomelanin).

The eumelanin structure is formed by aggregating the oligomer stacks driven by secondary interactions, such as hydrogen bonding.[35] High pH conditions disrupt the hydrogen bonding between oligomer stacks and lead to deaggregation [Fig. 1(a)]. Squid eumelanin was previously shown to be disassembled without chemical decomposition under deoxygenated alkaline conditions.[22] The average thickness of the squid subunits is shown to be ~1 nm, consistent with the dimension of eumelanin oligomer stacks that were previously determined by scanning tunneling microscopy and small-angle x-ray scattering.[35,36] However, Fig. 1(b) shows significant differences between sepia and squid eumelanin. As shown in Fig. 1(c), we also find that the subunits resulting from deaggregation of squid eumelanin are thinner than 3 nm, with an average thickness of 1.2 nm, and that the subunits obtained by deaggregation of sepia eumelanin are thinner; the thickness distribution of the resulting subunits is in a range of <1 nm.

The difference in thickness arises from the difference in the monomeric ratio between DHI and DHICA,[33] and is characterized in synthetic (Fig. S3, in the Supplementary Materials) and natural models. Oxidative decomposition of eumelanin in

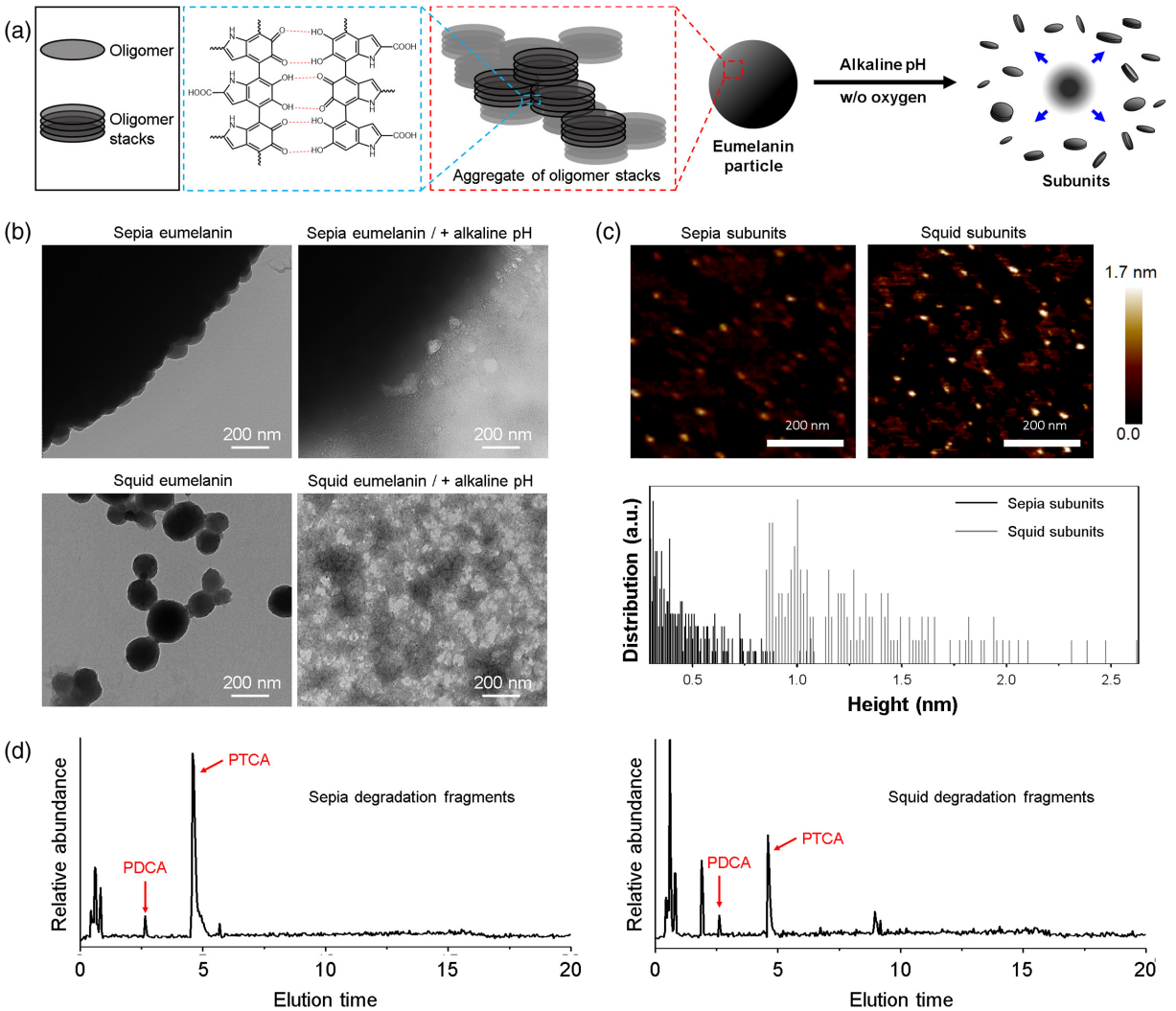

Fig. 1 Characterization of natural eumelanin models. (a) Schematic illustration of the self-assembled structure of eumelanin and deaggregation process induced by alkaline pH; (b) TEM images of sepia and squid eumelanin before and after exposure to alkaline pH condition in the absence of oxygen for 6 h. (c) AFM analysis of deaggregated subunits from sepia and squid eumelanin. Subunits obtained from deaggregation of sepia and squid eumelanin are deposited on a spinning mica substrate before analysis. (d) HPLC chromatograms of degradation products from sepia and squid eumelanin during alkaline hydrogen peroxide oxidation. PDCA and PTCA appear at 2.6 and 4.6 min, respectively.

alkaline hydrogen peroxide breaks the two eumelanin monomers (DHI and DHICA) into characteristic chemical markers, PDCA, and PTCA, respectively. Sepia eumelanin yields about 50-fold more PTCA than PDCA,[37] but HPLC analysis mediated by mass spectroscopy shows that the PTCA/PDCA ratio of squid eumelanin is significantly lower than that of sepia eumelanin [Fig. 1(d)], Figs. S4–S6, in the Supplementary Materials). This has structural consequences. The increased proportion of DHI would make the stacking between oligomers in squid melanin more favorable than in sepia eumelanin during the assembly process. Because oxidative oligomerization of DHI leads to planar oligomers, they tend to stack at the early stage of the multistep assembly process. Thus, DHI-derived eumelanin particles are formed by aggregates of highly stacked oligomers. In contrast, stacking between DHICA-derived oligomers will be restricted because their molecular structure is not planar but twisted. Therefore, DHICA-derived eumelanin particles can be regarded as the aggregates of thin oligomer stacks.

Natural melanin often contains many constituents, such as chelated metals. To verify whether the effects observed are due to the biopolymer, we also characterized subunits generated by disassembling the synthetic dopamine-derived eumelanin particles (dopamine-melanin), which forms DHI-rich structure,[33] and the DOPA(3–4 dihydroxyphenylalanine)-derived eumelanin particles (DOPA-melanin), which forms DHICA-rich structure. These are compared in Fig. S3, in the Supplementary Materials. The dopamine-derived subunits are also much thicker than those from DOPA, thus indicating that the chemical structure of eumelanin monomeric units is key for determining the aggregation mode.

3.2 *Aggregation Effect on the Pump-Probe Signal of Eumelanin Models*

Figure 2(a) shows the pump-probe signals for sepia and squid eumelanin obtained with 720 nm pump and variable probe (770 to 830 nm) as a function of interpulse delay time. Pump-probe signals of sepia and squid eumelanin are clearly different; sepia eumelanin particles exhibit positive-dominant signals, whereas the pump-probe signals of squid eumelanin particles are negative-dominant. HCl treatment did not eliminate these differences, which indicates that the different signal does not originate from possible metal–melanin complexes existing on the surface of natural eumelanin but arises from their intrinsic electronic features (Fig. S7, in the Supplementary Materials). In contrast, subunits generated by deaggregation of squid and sepia eumelanin particles show similar positive-dominant pump-probe signals. Thus, the pump-probe signals of squid eumelanin subunits change from positive- to negative-dominant with aggregation, whereas the pump-probe signals of sepia eumelanin subunits are not sensitive to aggregation.

The negative pump-probe signal of squid eumelanin (negative sign means that the probe laser is transmitted more strongly when the pump is on) can have multiple contributions, such as ground-state bleaching (GSB), stimulated Raman scattering (SRS), and stimulated emission (SE). Power studies show that the time-delayed positive signal can be assigned to excited-state absorption (ESA) that is linear in pump and in probe (Fig. S8, in the Supplementary Materials). So while some portions of the instantaneous negative signal could arise from the SRS for these differences between pump and probe wavelength, the Raman signal reflects bond-localized structure[38] and cannot explain the enormous difference that we observe in these large aggregates. In addition, SRS signals are confined to delays where pump and probe pulses still overlap, whereas the clearest difference between squid eumelanin particles and deaggregated subunits is observed in the time-delayed signal [Fig. 2(b)]. SE could contribute to the time-delayed negative signal of the squid eumelanin; melanin that was electronically excited by a pump pulse can be stimulated down to the ground state by a time-delayed probe pulse that matches the transition energy of spontaneous emission. However, squid eumelanin particles do not exhibit any appreciable spontaneous emission, whereas deaggregated subunits have shown clear spontaneous emission at a broad range of UV and visible wavelengths.[22] Based on the observed spontaneous emission, the possible SE signal of eumelanin particles should be lower than in the deaggregated subunits; however, this is not seen in the experiments. In addition, isolated subunits did not show any spontaneous emission that matches the probe energy, when excited by wavelengths longer than 700 nm (Fig. S9, in the Supplementary Materials). Therefore, it is reasonable to expect that simulated emission does not significantly contribute to the aggregation-dependent pump-probe signal of squid eumelanin.

Hence, we conclude that the time-delayed negative signal of squid eumelanin is mainly attributed to GSB. Power studies for squid eumelanin have shown that GSB signal is also linear in pump and in probe. (Figs. S10 and S11, in the Supplementary Materials). GSB signal is observed when both pump and probe are in resonance with the chromophore band. Eumelanin exhibits unique monotonic broadband absorption that is explained by the combination of various chromophore bands with different HOMO-LUMO gaps. If chromophore bands in the near-IR region are broad enough to be in resonance with both pump and probe, eumelanin will give rise to the GSB signal. The aggregation-dependent signal change from ESA- to GSB-dominant signal can be explained by the generation of a broad charge–transfer band arising from quinhydrone formation. Melanin pigment contains many quinone and quinol groups; these units will be present within the eumelanin self-assembled structure as quinhydrone or other quinone–quinol complexes.[39,40] These complexes[41] generate broad charge–transfer absorption bands, leading to enhanced GSB. Highly stacked oligomers should have a geometric preference that allows their lateral faces to be linked together more efficiently, thereby generating intense charge–transfer bands, which would weaken with decreased stacking. Hence, we attribute ESA-dominant signals (not sensitive to deaggregation) in sepia eumelanin to low geometric packing preference, whereas we attribute GSB-dominant signals (changing to ESA upon deaggregation) in squid eumelanin to the relatively high extent of stacking in the assembled subunits [Fig. 2(c)]. A confirmation of this interpretation is provided by synthetic melanins; pump-probe signals of dopamine-melanin are highly sensitive to deaggregation, but those of DOPA-melanin are not sensitive to deaggregation (Fig. S12, in the Supplementary Materials).

The positive-dominant signals in Fig. 2 for sepia eumelanin subunits seem to contradict a previous study[7] that observed a long-lived negative (GSB-dominant) signal in the size-selected fraction of sepia eumelanin smaller than 3 kDa. We attribute this difference to the method of preparation. In Ref. 7, the size-selected fraction of small sepia eumelanin particles was obtained by filtration after centrifugation. The small oligomeric species thus were likely physically absorbed on the surface of larger particles, and could easily be affected by even small amounts of residual iron.[7] Even though treatment with a chelator

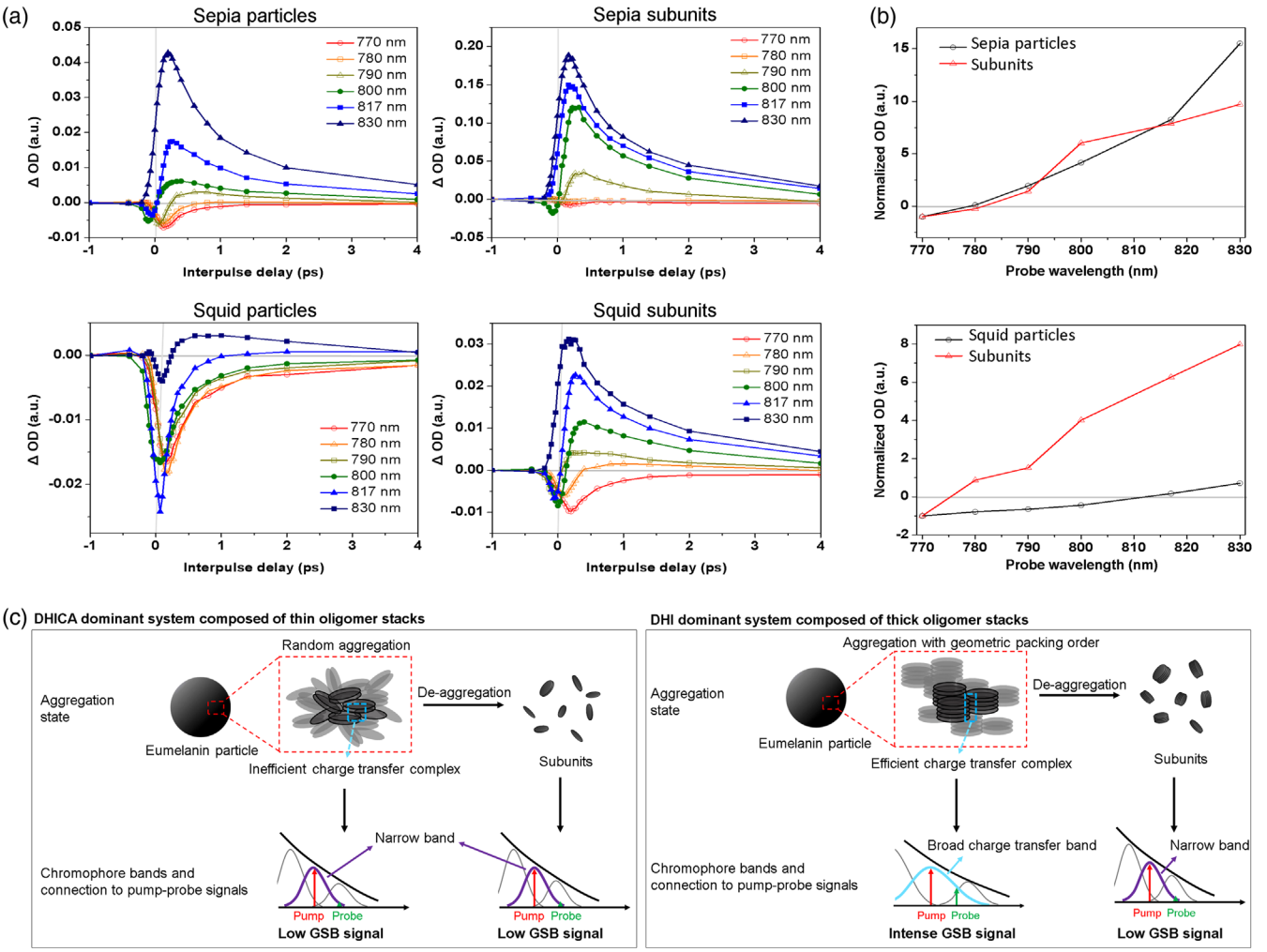

Fig. 2 Effect of aggregation on pump-probe signal of eumelanin: (a) 720 nm pump and variable probe signal of eumelanin models and their subunits obtained from deaggregation process under deoxygenated alkaline condition. (b) Time-delayed transient signal at 2 ps as a function of probe wavelength. Signal is normalized at 770 nm. (c) Schematic summary of the proposed relationship between the aggregation-dependent chromophore band of eumelanin and the resulting pump-probe signal. Sepia eumelanin particles, with thin oligomer stacks, do not lead to the efficient edge-to-edge interaction because of low geometric packing preference between oligomer stacks in large-scale aggregation system. Thus, eumelanin particles formed by aggregation of thin oligomer stacks show very similar chromophore bands with their subunits. Because chromophore bandwidth for sepia eumelanin is not broad enough to be in resonance with both pump and probe, GSB is negligible and the whole signal is dominated by ESA. In contrast, squid eumelanin is formed by aggregating the thick oligomer stacks. Because of the high geometric packing preference when aggregated, efficient generation of charge–transfer complexes at the edge of oligomer stacks is possible. Aggregation will result in broad charge–transfer bands that can be resonant with both pump and probe, and thus will lead to intense GSB signal. Because broad charge–transfer bands disappear with deaggregation, GSB signals observed in squid eumelanin particles also diminish with deaggregation, resulting in ESA-dominant signals.

such as EDTA can remove much of the iron content in sepia eumelanin, about 10% of pre-existing Fe ions remain,[42] resulting in a negative pump-probe signal. In contrast, subunits resulting from pH-controlled dissociation of self-assembly structure in this study would not be sensitive to pre-existing Fe ions because a much greater portion of iron-free subunits is generated from inside of particles.

3.3 *Connection of the Signal of Eumelanin to Self-Assembly Structure*

Pump-probe microscopy has provided molecular information about the pigment distribution in melanoma, which is highly related to its metastatic potential.[5,12] In these studies, the most pronounced feature of pigmented skin lesions was that the ratio between GSB- and ESA-dominant signals is correlated with metastatic potential of melanoma. As shown in Fig. 3, eumelanin in black hair and benign black nevi exhibits GSB-dominant signals (green color), whereas ESA-dominant signals (red color) increase with high metastatic potential (as classified by positive SLNB results).

Based on these results, we examine two possible explanations. In melanomas, DCT is highly expressed in most primary tumors and cell lines.[32] In terms of molecular basis of eumelanin, DCT results in a DHICA-dominant eumelanin structure. Chemical analysis studies also show a high level of DHICA-

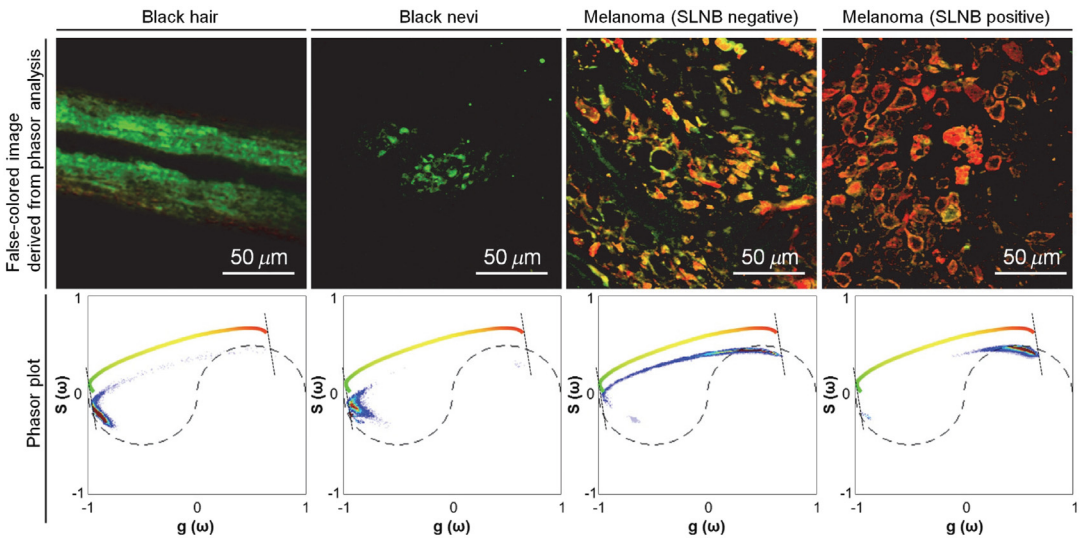

Fig. 3 Comparison of 720-nm pump/817-nm probe wavelength images between normal eumelanin (black hair and black nevi) and pigment distributed in melanoma (SLNB-positive and -negative). The false-colored images of black hair, black nevi, and melanoma (SLNB-positive and -negative) are derived from the phasor analysis shown in the bottom row. The color bar within the phasor plot denotes the color scheme used for the false-colored images. These single images are representative; much larger published datasets give the same general result, i.e., a shift from negative-dominant to positive-dominant with greater clinical concern.[5,12]

derived eumelanin in melanoma.[29,30] Therefore, it can be expected that the increased production of DHICA-derived eumelanin mediated by DCT contributes to ESA-dominant signals of melanoma.

A second factor relating to the pump-probe signals in melanoma is the dissociation of DHI-derived eumelanin. Dissociation is a pronounced feature found in pigmented skin lesions, and its rate is related to metastatic potential.[24,25,43] Because small fragments generated by deaggregation of DHI-derived eumelanin exhibit ESA-dominant signals, dissociation of the eumelanin particle structure could contribute to an increase in the time-delayed positive signal, as validated by the cellular uptake experiment in Fig. 4. Disintegration of melanosomes has been repeatedly observed in membrane-enclosed lysosomal compartments (such as autophagosomes and heterophagosomes) in cells, including macrophages and melanoma cells.[44–47] Three types of cells—melanoma cells (B16), breast cancer (4T1), and macrophage (RAW 264.7) cells—were incubated with squid eumelanin particles for 14 h. As shown in Fig. 4, the two melanin-free cell lines show heterogeneous melanin signals after cellular uptake, reflecting the expected structural dissociation in lysosomal compartments. B16 melanoma, of course, also has a melanin background (Fig. S13, in the Supplementary Materials) but the signals are clearly different from the intense heterogeneous signals after cellular uptake of squid eumelanin.

Clear evidence for structural disintegration was observed by TEM. As shown in TEM images of thin slides after cellular uptake [Fig. 4(g)], it appeared that the particles internalized in cells were localized in vesicles (most likely lysosomes in 4T1 cells and phagolysosomes in RAW 264.7 cells) and exhibited clear structural alterations. Many of the internalized squid eumelanin particles exhibited heterogeneous density and amorphous shape at the edges. The particles were co-localized with other amorphous components. These findings clearly indicated that squid eumelanin underwent structural disintegration in the vesicles, resulting in the predominant ESA signals in the lysosomal compartment.

Histological studies have repeatedly described that structural alteration of melanin pigment is observed in phagosomes.[48,49] Melanin is hardly dissociated by the hydrolytic mechanism of lysosomal enzymes,[50] but melanin structure is sensitive to oxidative stress, for example, due to the presence of hydrogen peroxide.[51–53] This suggests that melanin is oxidatively degraded by phagosomal enzyme activity.[54] Hydrogen peroxide is a strong candidate for causing the oxidative degradation because it is not only produced by phagosomal enzyme activity but also generated during melanin synthesis as a by-product.[55] In this regard, we compared susceptibility to oxidative degradation between two eumelanin models by exposing them to hydrogen peroxide solution. Figure S14 in the Supplementary Materials section shows the time-course TEM images of sepia and squid eumelanin after exposure to hydrogen peroxide (28%) under dark conditions. Squid eumelanin exhibits only slight morphological modifications on the particle surface even after exposure for 16 h. Even though a small portion of particles shows amorphous feature, most retain their spherical character. In contrast, the morphology of sepia eumelanin appears to be significantly changed after exposure to hydrogen peroxide for 16 h. We would thus argue that the increase in DHICA content in melanomas also increases susceptibility to degradation. This is verified again with synthetic models, using dopamine- or racemic DOPA-derived melanin particles (Fig. S14, in the Supplementary Materials); synthetic eumelanin particles derived from oxidation of dopamine or racemic DOPA show squid or sepia eumelanin-like structural features, respectively. It has been proposed that bleaching of eumelanin by hydrogen peroxide is caused by a two-step process: reversible oxidation of hydroquinone moiety leading to quinone units and irreversible ring opening of the quinone group by nucleophilic attack of OOH^- ions.[51] In this picture, one- or two-electron oxidation processes for hydroquinone

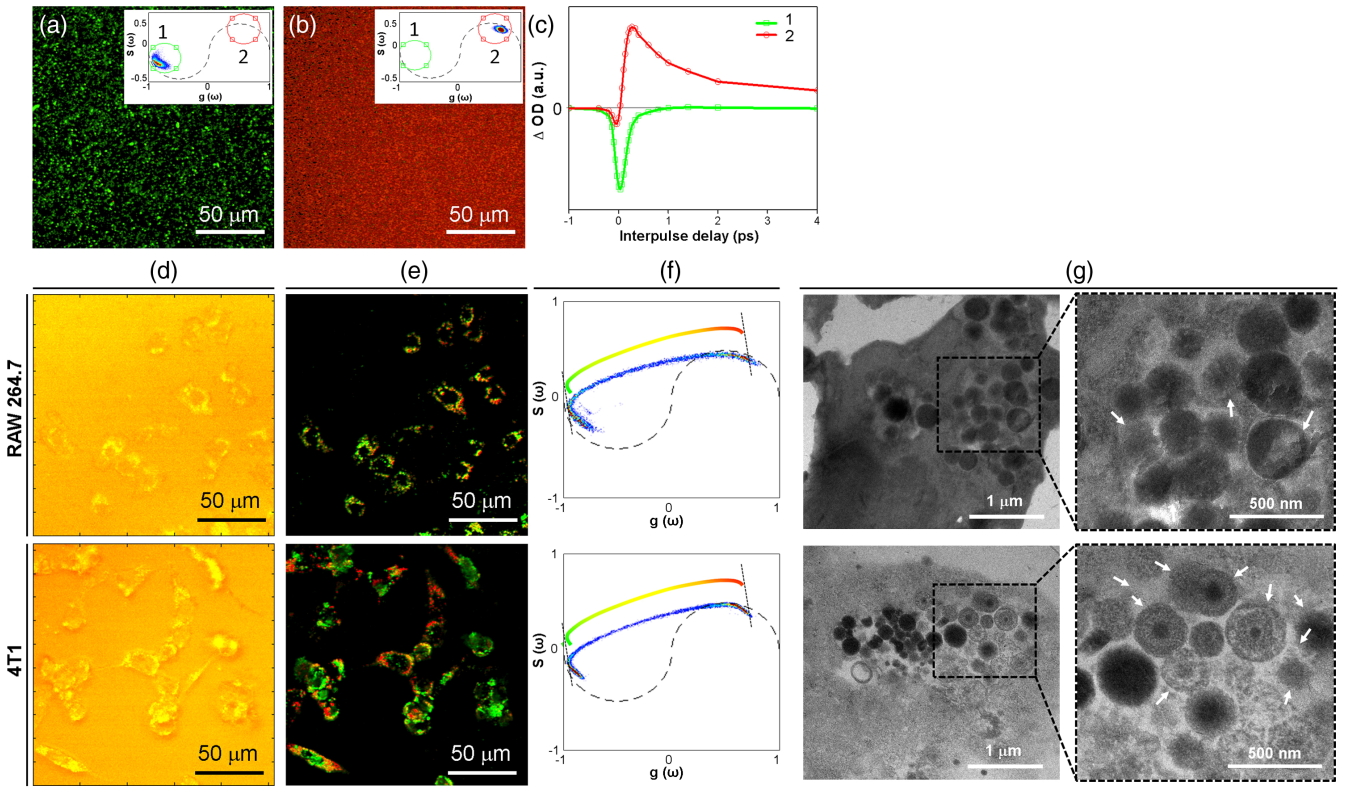

Fig. 4 Structural dissociation of squid eumelanin induced by cellular uptake. False-color images of (a) squid eumelanin particles and (b) deaggregated subunits derived from phasor analysis. Inset shows the phasor distribution for each sample. Samples are dispersed in agarose gel. From the phasor distribution, we have assigned false colors to two different regions, circles 1 and 2. (c) TA signal is shown corresponding to the phasor distributions 1 and 2 shown in (a) and (b). (d) Confocal images of RAW 264.7 and 4T1 cells after incubation with squid eumelanin particles for 14 h. (e) False-color images are shown of cells derived from phasor analysis shown in (f). (f) Phasor distribution of each sample. The color bar within the figure denotes the color scheme used for the images in (e). (g) TEM images of squid eumelanin particles internalized in RAW 264.7 and 4T1 cells. Arrows indicate squid eumelanin particles exhibiting structural disintegration inside each cell.

group are important for the generation of quinone groups. Considering the self-assembly structure of eumelanin, quinhydrone complex formation would decrease the reaction rate for reversible oxidation of the hydroquinone group in the eumelanin-bleaching process. Therefore, the high structural robustness against oxidative degradation of DHI-derived eumelanin may originate from their numerous quinhydrones, as well as the compact pi-stacking and aggregation structure leading to restricted accessibility of OOH-ions.

The tremendous strength of pump-probe microscopy is the large number of adjustable parameters that can be used to enhance the contrast. Figures 5 and 6 present data with a completely different set of wavelengths (770-nm pump, 730-nm probe) where the decay curves are drastically altered; the signals are always negative (meaning more probe light gets transmitted when the pump is on), but the lifetime is sensitive to dissociation of the eumelanin self-assembly structures. For this wavelength combination, bulk sepia and squid eumelanin particles are nearly indistinguishable, yet it retains the ability to distinguish between benign, non-metastatic, and metastatic cancers (Fig. 5). This implies that the molecular-level diagnostic driver in these images (and at least the dominant component in Fig. 3) is the dissociation of the self-assembly structure.

As noted earlier, with the 720/817 nm combination (or close wavelengths), there is also a signal sign difference between eumelanin and pheomelanin, which was originally assumed to be the source of the image difference.[5] Figure 6 proves that this is not the clinically relevant interpretation, because pheomelanin and eumelanin give very different lifetimes with the 770/730 nm wavelength combination, and that tissue can be assigned unambiguously to having the observed pump-probe signal from eumelanin alone.

3.4 *Biological Implications of DHICA-Derived Eumelanin*

Figure 7 represents the proposed relationship between eumelanin self-assembly structure, function, and pump-probe signal in pigmented skin lesions based on the discovery made in this study. Melanoma cells have low catalase activity and glutathione levels,[56] indicating that they have a weak defense system against oxidative stress. Therefore, the imbalance of redox homeostasis, caused by a decrease in the antioxidant system and an increase in ROS level by phagosomal enzyme activity, would expose eumelanin pigment to high levels of oxidative stress. In this stage, DHI-dominant eumelanin, with high structural robustness against oxidative stress, would not easily deaggregate into fragments. This aspect changes with an increase in the DCT level. High expression levels of DCT in melanoma increase the level of DHICA-derived eumelanin, which is highly susceptible to

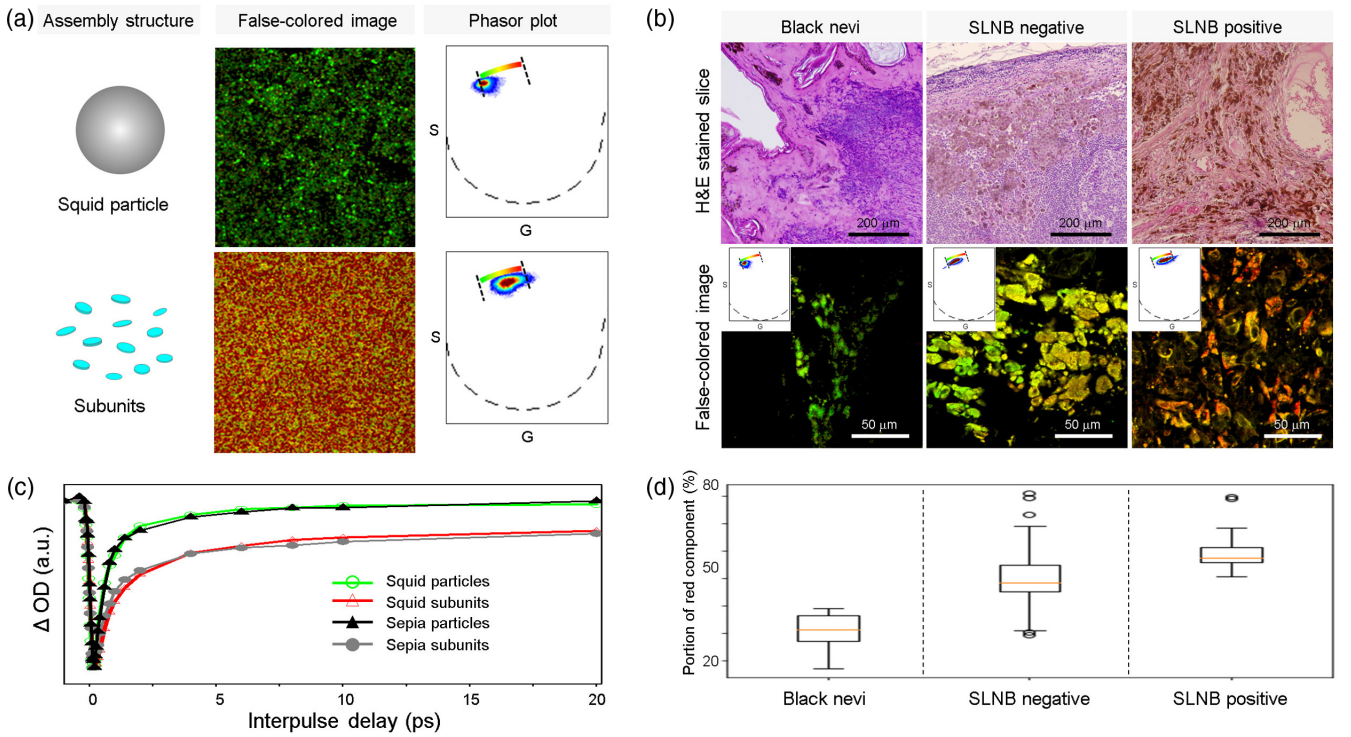

Fig. 5 The 770-nm pump/730-nm probe signals of eumelanin and correlation with melanoma. (a) Images of squid eumelanin particles with different assembly state. The small subunit fraction (MW < 2 KDa) resulting from disassembly of squid eumelanin particles can be differentiated by phasor analysis. At this wavelength, all signals are negative, so all phasors have $-1 < g < 0$ and only the left side is plotted. Note that the small subunit fraction is hardly observed in 720-nm pump/817-nm probe experiments but is clearly observed here. (b) Pump-probe images in benign nevi and melanoma. The false-colored images derived from phasor analysis showed that chemical heterogeneity and the amount of long-lived positive signal increases with development and metastasis of melanoma, reflecting that dissociation of eumelanin increases with elevated risk of metastasis. Images in the upper row are H&E-stained slices. (c) Pump-probe delay curves for squid and sepia eumelanin particles and their disassembled subunits, showing that the difference between DHI and DHICA does not contribute to the observed signals at this wavelength. (d) Boxplots showing the content of the highly dissociated fragments (the red component) for benign nevi ($n = 3$, 9 images total), primary melanomas ($n = 11$, 59 images total), and metastatic melanomas ($n = 5$, 29 images total). There is a highly significant difference in the content of the long-lived component among these three disease states (type II 2-factor ANOVA for classification versus case ID, $p < 2 * 10^{-14}$).

oxidative dissociation, and therefore hastens the disintegration of melanin into small fragments. Extremely high levels of ROS can induce cell apoptosis; with very low level of ROS, proliferation will not be efficient. Therefore, a sustainable and adequate level of ROS is a key to efficient progression of most cancer cells[57] and could be maintained by the high photochemical reactivity of the resulting small eumelanin fragments. Considering that ROS can serve as the key signaling molecules for melanoma proliferation and metastasis,[57] high levels of DCT may be involved in the regulation of eumelanin function during malignant transformation of melanoma.

4 Discussion

Assignment of a physical basis to the observed signal, and thus a correlation between the biochemistry and the pump-probe image structure, is valuable for understanding how to optimize sensitivity to address important clinical questions, such as the metastatic potential of excised tumors. The one-sentence, oversimplified version of our results is that dissociation of the eumelanin assembly structure, induced by metabolic activity of cancers, is the dominant molecular mechanism behind the clinically important feature, chemical heterogeneity of the pump-probe signals in metastatic melanoma. These changes are essentially invisible in conventional absorption microscopy, but clearly seen in the pump-probe images. This connection among cellular chemistry, clinical outcome, and straightforward imaging methods implies that pump-probe microscopy has great potential to improve patient outcomes. For example, the recent development of monoclonal antibodies ("checkpoint inhibitors")[58] that block inhibitory pathways in the human immune system offers the potential for effective use of adjuvant therapies on potentially aggressive tumors, if they can be identified in early stages.

Eumelanin has long been among the most mysterious biomolecules in terms of its structure–property–function relationship because of its high structural complexity and conflicting behaviors. Therefore, our approach to give molecular contrast in eumelanin by visualization with pump-probe microscopy provides a potential platform for studying the physiological significance of eumelanin self-assembly structure in various biological systems. Structural dissociation of melanin pigment is relevant

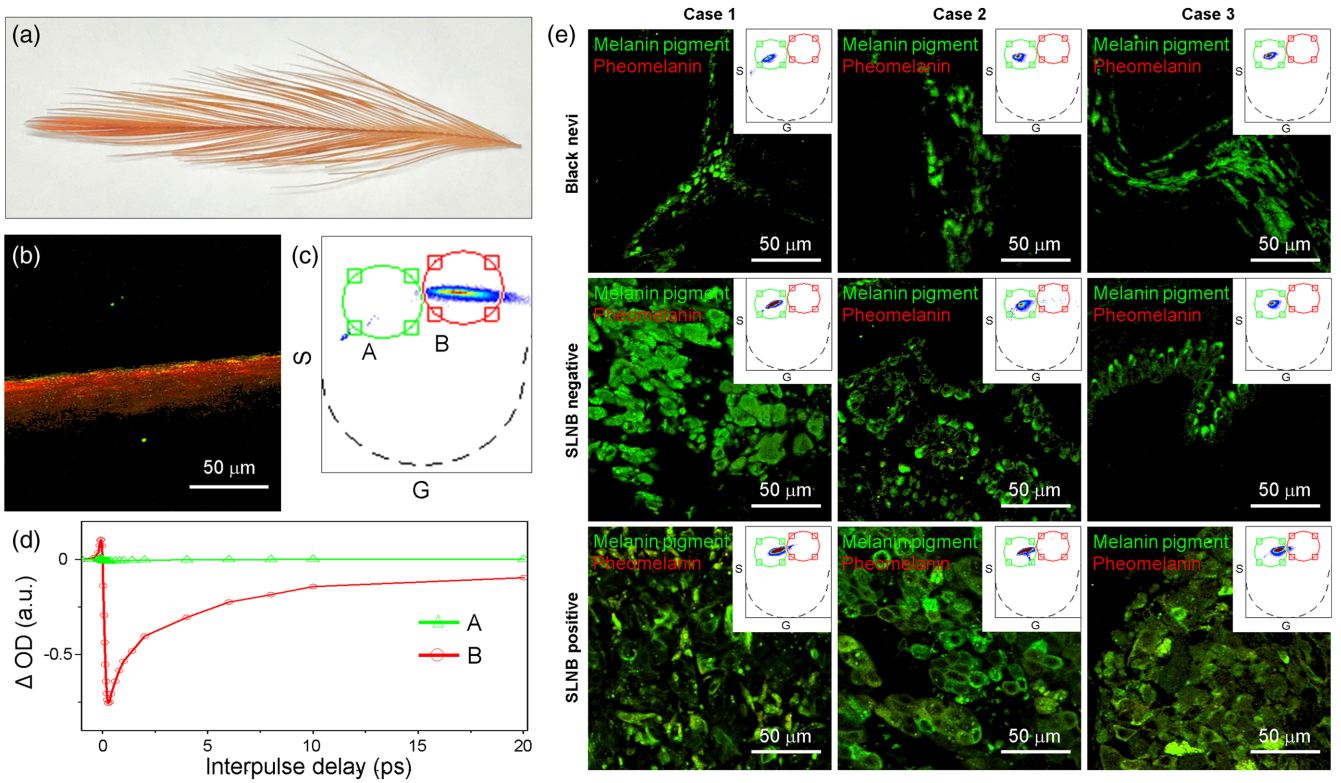

Fig. 6 Characterization of pheomelanin and its contribution to pigmentation in black nevi, primary melanoma, and metastatic melanoma using 770 nm pump/730 nm probe imaging. (a) Picture of red chicken feather. (b) False-colored images of pheomelanin in red chicken feather derived from (c) the phasor analysis. (d) Pump-probe signal corresponding to regions A and B in the phasor plot (c). Region A corresponds to the signal distribution of eumelanin with different assembly states. Most pump-probe signals of pheomelanin are observed in region B, which clearly differs from that of eumelanin in Fig. 5. (e) Contribution of pheomelanin to pigmentation in black nevi, primary melanoma, and metastatic melanoma. The red component (corresponding to pheomelanin signals) is negligible in all samples.

to other pigment-related diseases, such as Parkinson's disease and age-related macular degeneration. In combination with conventional chemical analysis methods, pump-probe microscopy probing molecular details of eumelanin pigment can be widely applied in studies relating to the deleterious role of pigment in the process of age-related diseases.

5 Methods

5.1 *Emission Spectra of Deaggregated Subunits*

Emission spectra of the deaggregated subunits were recorded by a spectrofluorometer (Fluorolog-3, HORIBA). For the emission spectra, deaggregated subunits solution was highly diluted and excited by variable wavelength (400 to 750 nm).

5.2 *Preparation of Synthetic Melanin Models*

Dopamine-melanin particles were prepared through spontaneous oxidation of dopamine, as described in a previous report.[59] About 180 mg of dopamine hydrochloride was dissolved in 90 mL deionized water. A NaOH solution (780 μL, 1 N) was added to the solution of dopamine hydrochloride under vigorous stirring at room temperature. After 5 h, dopamine-melanin particles were retrieved via centrifugation (19,000 rpm for 10 min) and purified with sequential centrifugation (19,000 rpm for 10 min) and re-dispersion in deionized water for three times. Morphological shape of prepared dopamine-melanin was characterized by TEM. DOPA-melanin was prepared, as described in a previous report, with slight modification.[60] About 70 mg of L-DOPA was dissolved in deionized water (50 mL) by heating. $KMnO_4$ solution (280 μL, 1 N) was added to the solution of L-DOPA under vigorous stirring at room temperature. After 8 h, DOPA-melanin were retrieved via centrifugation (20,000 rpm for 10 min) and dispersed in deionized water. DOPA-melanin was purified with sequential centrifugation (20,000 rpm for 10 min) and re-dispersion in deionized water for three times. To remove the Mn^{2+} ions present in DOPA-melanin, DOPA-melanin suspension was incubated in HCl solution (4 N) for 24 h. After HCl treatment, DOPA-melanin particles were retrieved by centrifugation and re-dispersed in deionized water. DOPA-melanin were purified with sequential centrifugation (20,000 rpm for 10 min) and re-dispersion in deionized water for three times. The pH-controlled disassembly process, which was described in the case of natural eumelanin models, was applied to induce the disassembly of synthetic melanin models.

5.3 *Surface Modification of Squid Eumelanin Particles*

Before the cellular uptake experiment, squid eumelanin particles were treated with polyvinylpyrrolidone (PVP) for enhancement of dispersion stability in cell culture medium. About 5 mg of

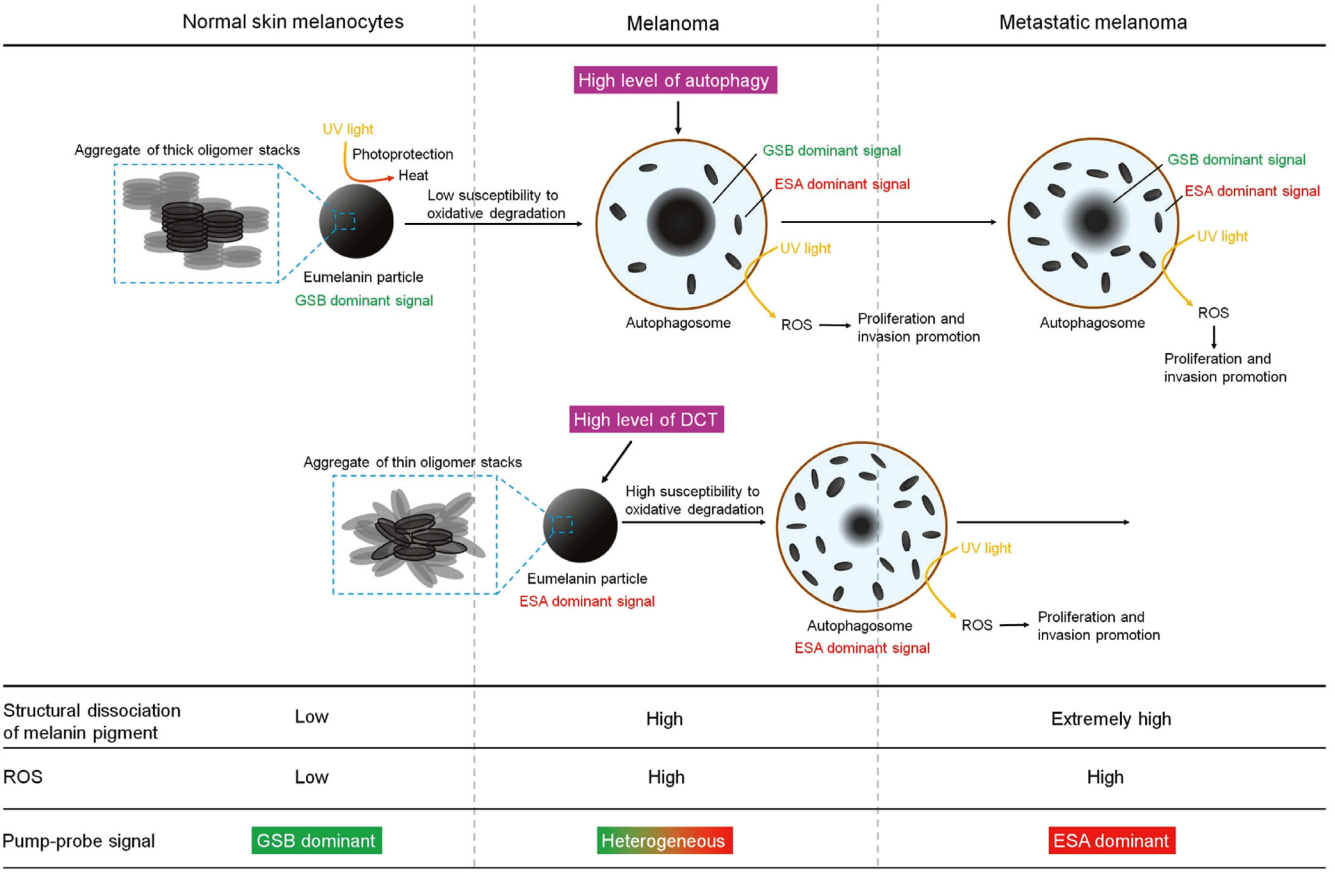

Fig. 7 Proposed model for the chemical heterogeneity of eumelanin in the progression of melanoma and its relation to the pump-probe signal. Eumelanin formed by aggregation of thick oligomer stacks is primarily distributed in normal melanocytes. In this stage, the pump-probe signal of normal melanocyte is dominated by GSB. With the development of melanoma, the pigment experiences structural dissociation in lysosomal compartments such as autophagosomes and heterophagosomes. The structural alteration leads to small subunit fragments and makes the pump-probe signal heterogeneous, but this process is not effective because of its low susceptibility to oxidative degradation in the lysosomal compartments. On the other hand, population of eumelanin formed by aggregation of thin oligomer stacks (DHICA-derived eumelanin) increases with high level of DCT in melanoma. Because eumelanin composed of thin oligomer stacks is very susceptible to oxidative degradation, a large portion of newly generated eumelanin in melanoma undergoes structural dissociation. Small eumelanin fragments are shown to have a high capability to generate ROS. Thus, the structural dissociation of eumelanin leads to an increase in ROS levels, serving as signaling molecules for the promotion of melanoma proliferation and metastasis. In this phase, ESA signal is highly increased because of the generation of eumelanin formed by aggregate of thin oligomer stacks and small fragments. In metastatic melanoma, the high level of autophagy and eumelanin sensitive to oxidative degradation allows most of the pigmentation to be dissociated into small subunit fragments. Thus, pump-probe signals of metastatic melanomas are dominated by ESA.

PVP (Sigma Aldrich, 360 K) was added to 10 mL of squid eumelanin (1 mg/mL, water). After vigorous shaking, they were purified by consecutive centrifugation (20,000 rpm, 10 min) and redispersed in water for four times. After the treatment with PVP, squid eumelanin particles did not show appreciable morphological change (Fig. S15, in the Supplementary Materials).

5.4 *Statistical Analysis of Pump-Probe Images*

To quantify the chemical composition of each image, we took the ratios of the sum of the intensities in both channels (red and green), and plotted these ratios in boxplots [Fig. 3(c)]. To test for statistical significance, we ran a two-factor type II ANOVA test, where the two factors were (1) the sample number (whether the images come from the same sample), and (2) the class [whether the samples are black nevi, primary melanoma (SLNB-negative), or metastatic melanoma (SLNB-positive)]. The first factor was necessary to account for the difference in chemical content due to sample-to-sample variation, which was not of interest. The test returned a p-value of 1.2×10^{-14}, thus decisively suggesting that there was a significant difference in chemical composition among the three classes.

5.5 *Susceptibility of Eumelanin Models against Oxidative Degradation*

About 500 μL of 30% H_2O_2 solution was added to 200 μL of melanin suspension (1 mg/mL) to induce oxidative degradation of melanin. Morphological changes of melanin particles were monitored by TEM after exposure to H_2O_2 solution. To rule out

the light-mediated oxidation process, oxidation of melanin particles was induced in the dark. Before TEM analysis, melanin particles were centrifuged and re-dispersed in water twice to remove H_2O_2 in the solution. Degradation kinetics of melanin particles was determined by measuring the absorption of small fragments that were released from parental melanin particles in H_2O_2 solution as a function of time. Because small oxidation fragments released from melanin particles were stably solubilized in the solution even after high-speed centrifugation, oxidation kinetics of melanin particles in H_2O_2 solution was monitored by measuring the absorption of supernatant after centrifugation (14,000 rpm, 15 min). To rule out Fenton-like reactions on the surface of eumelanin particles, all melanin models were incubated in 4 M HCl solution for 24 h. After the HCl treatment, melanin models underwent sequential centrifugation and re-dispersion in water for three times.

Disclosures

The authors declare that there are no conflicts of interest related to this article.

Acknowledgments

We thank Francisco Robles and Jesse Wilson for their help in various stages of this work. This work was funded by the National of Institutes of Health under Grant No. R01 CA166555 and by the National Science Foundation under Grant No. CHE-1610975.

References

1. D. C. Whiteman, P. D. Baade, and C. M. Olsen, "More people die from thin melanomas (1 mm) than from thick melanomas (>4 mm) in Queensland, Australia," *J. Invest. Dermatol.* **135**(4), 1190–1193 (2015).
2. S. M. Landow, A. Gjelsvik, and M. A. Weinstock, "Mortality burden and prognosis of thin melanomas overall and by subcategory of thickness, SEER registry data, 1992–2013," *J. Am. Acad. Dermatol.* **76**(2), 258–263 (2017).
3. P. A. Gimotty et al., "A population-based validation of the American Joint Committee on cancer melanoma staging system," *J. Clin. Oncol.* **23**(31), 8065–8075 (2005).
4. M. F. Kalady et al., "Thin melanomas: predictive lethal characteristics from a 30-year clinical experience," *Ann. Surg.* **238**(4), 528–535 (2003).
5. T. E. Matthews et al., "Pump-probe imaging differentiates melanoma from melanocytic nevi," *Sci. Transl. Med.* **3**(71), 71ra15 (2011).
6. J. W. Wilson et al., "Comparing in vivo pump-probe and multiphoton fluorescence microscopy of melanoma and pigmented lesions," *J. Biomed. Opt.* **20**(5), 051012 (2015).
7. M. J. Simpson et al., "Near-infrared excited state dynamics of melanins: the effects of iron content, photo-damage, chemical oxidation, and aggregate size," *J. Phys. Chem. A* **118**(6), 993–1003 (2014).
8. T. E. Matthews et al., "In vivo and ex vivo epi-mode pump-probe imaging of melanin and microvasculature," *Biomed. Opt. Express* **2**(6), 1576–1583 (2011).
9. J. W. Wilson et al., "Imaging microscopic pigment chemistry in conjunctival melanocytic lesions using pump-probe laser microscopy," *Invest. Ophthalmol. Visual Sci.* **54**(10), 6867–6876 (2013).
10. F. E. Robles, J. W. Wilson, and W. S. Warren, "Quantifying melanin spatial distribution using pump-probe microscopy and a 2-D morphological autocorrelation transformation for melanoma diagnosis," *J. Biomed. Opt.* **18**(12), 120502 (2013).
11. F. E. Robles et al., "Label-free imaging of female genital tract melanocytic lesions with pump-probe microscopy: a promising diagnostic tool," *J. Lower Genit. Tract Dis.* **21**(2), 137–144 (2017).
12. F. E. Robles et al., "Pump-probe imaging of pigmented cutaneous melanoma primary lesions gives insight into metastatic potential," *Biomed. Opt. Express* **6**(9), 3631–3645 (2015).
13. R. Marchesini, A. Bono, and M. Carrara, "In vivo characterization of melanin in melanocytic lesions: spectroscopic study on 1671 pigmented skin lesions," *J. Biomed. Opt.* **14**(1), 014027 (2009).
14. G. Zonios et al., "In vivo optical properties of melanocytic skin lesions: common nevi, dysplastic nevi and malignant melanoma," *Photochem. Photobiol.* **86**(1), 236–240 (2010).
15. M. J. Simpson et al., "Pump-probe microscopic imaging of Jurassic-aged eumelanin," *J. Phys. Chem. Lett.* **4**(11), 1924–1927 (2013).
16. E. Kvam and R. M. Tyrrell, "The role of melanin in the induction of oxidative DNA base damage by ultraviolet A irradiation of DNA or melanoma cells," *J. Invest. Dermatol.* **113**(2), 209–213 (1999).
17. S. Takeuchi et al., "Melanin acts as a potent UVB photosensitizer to cause an atypical mode of cell death in murine skin," *Proc. Natl. Acad. Sci. U.S.A.* **101**(42), 15076–15081 (2004).
18. D. Barker et al., "Comparison of the responses of human melanocytes with different melanin contents to ultraviolet B irradiation," *Cancer Res.* **55**(18), 4041–4046 (1995).
19. B. L. Seagle et al., "Time-resolved detection of melanin free radicals quenching reactive oxygen species," *J. Am. Chem. Soc.* **127**(32), 11220–11221 (2005).
20. C. M. Clancy and J. D. Simon, "Ultrastructural organization of eumelanin from Sepia officinalis measured by atomic force microscopy," *Biochemistry* **40**(44), 13353–13360 (2001).
21. F. H. M. de Melo, F. Molognoni, and M. G. Jasiulionis, "The role of oxidative stress in melanoma development, progression and treatment," Chapter 5 in *Recent Advances in the Biology, Therapy and Management of Melanoma*, L. M. Davids, Ed., InTech, Rijeka, Croatia, pp. 83–110 (2013).
22. K. Y. Ju et al., "Clue to understanding the janus behavior of eumelanin: investigating the relationship between hierarchical assembly structure of eumelanin and its photophysical properties," *Biomacromolecules* **17**(9), 2860–2872 (2016).
23. M. Zareba et al., "Effects of photodegradation on the physical and antioxidant properties of melanosomes isolated from retinal pigment epithelium," *Photochem. Photobiol.* **82**(4), 1024–1029 (2006).
24. A. R. Rhodes et al., "Melanosomal alterations in dysplastic melanocytic nevi. A quantitative, ultrastructural investigation," *Cancer* **61**(2), 358–369 (1988).
25. R. C. Curran and B. G. McCann, "The ultrastructure of benign pigmented naevi and melanocarcinomas in man," *J. Pathol.* **119**(3), 135–146 (1976).
26. L. Panzella et al., "Atypical structural and pi-electron features of a melanin polymer that lead to superior free-radical-scavenging properties," *Angew. Chem. Int. Ed. Engl.* **52**(48), 12684–12687 (2013).
27. L. Ascione et al., "Intermolecular pi-electron perturbations generate extrinsic visible contributions to eumelanin black chromophore in model polymers with interrupted interring conjugation," *Photochem. Photobiol.* **89**(2), 314–318 (2013).
28. R. Xu et al., "An electrochemical study of natural and chemically controlled eumelanin," *APL Mater.* **5**, 126108 (2017).
29. T. G. Salopek et al., "Dysplastic melanocytic nevi contain high levels of pheomelanin: quantitative comparison of pheomelanin/eumelanin levels between normal skin, common nevi, and dysplastic nevi," *Pigm. Cell Res.* **4**(4), 172–179 (1991).
30. G. Odh et al., "Melanins in IGR 1 melanoma cells," *Pigm. Cell Res.* **7**(6), 419–427 (1994).
31. A. Wilczek, H. Kondoh, and Y. Mishima, "Composition of mammalian eumelanins: analyses of DHICA-derived units in pigments from hair and melanoma cells," *Pigm. Cell Res.* **9**(2), 63–67 (1996).
32. B. J. Pak and Y. Ben-David, "From melanocytes to melanoma," in *From Melanocytes to Melanoma: The Progression to Malignancy*, V. J. Hearing and S. P. L. Leong, Eds., Humana Press, Totowa, New Jersey, p. 577 (2006).
33. S. Ito and K. Wakamatsu, "Chemical degradation of melanins: application to identification of dopamine-melanin," *Pigm. Cell Res.* **11**(2), 120–126 (1998).
34. M. R. Chedekel, B. L. Murr, and L. Zeise, "Melanin standard method: empirical formula," *Pigm. Cell Res* **5**(3), 143–147 (1992).
35. K. C. Littrell et al., "Structural studies of bleached melanin by synchrotron small-angle x-ray scattering," *Photochem. Photobiol.* **77**(2), 115–120 (2003).

36. G. W. Zajac et al., "The fundamental unit of synthetic melanin: a verification by tunneling microscopy of x-ray scattering results," *Biochim. Biophys. Acta* **1199**(3), 271–278 (1994).
37. W. C. Ward et al., "Quantification of naturally occurring pyrrole acids in melanosomes," *Photochem. Photobiol.* **84**(3), 700–705 (2008).
38. Z. W. Huang et al., "Raman spectroscopy of in vivo cutaneous melanin," *J. Biomed. Opt.* **9**(6), 1198–1205 (2004).
39. C. C. Felix et al., "Interactions of melanin with metal ions. Electron spin resonance evidence for chelate complexes of metal ions with free radicals," *J. Am. Chem. Soc.* **100**(12), 3922–3926 (1978).
40. R. Arnaud et al., "Electron spin resonance of melanin from hair. Effects of temperature, pH and light irradiation," *Photochem. Photobiol.* **38**(2), 161–168 (1983).
41. J. Regeimbal et al., "Disulfide bond formation involves a quinhydrone-type charge—transfer complex," *Proc. Natl. Acad. Sci. U.S.A.* **100**(24), 13779–13784 (2003).
42. Y. Liu et al., "Ion-exchange and adsorption of Fe(III) by Sepia melanin," *Pigm. Cell Res.* **17**(3), 262–269 (2004).
43. J. Borovansky, P. Mirejovsky, and P. A. Riley, "Possible relationship between abnormal melanosome structure and cytotoxic phenomena in malignant melanoma," *Neoplasma* **38**(4), 393–400 (1991).
44. Y. Mishima, "Cellular and subcellular differentiation of melanin phagocytosis and synthesis by lysosomal and melanosomal activity," *J. Invest. Dermatol.* **46**(1), 70–75 (1966).
45. R. Lazova, V. Klump, and J. Pawelek, "Autophagy in cutaneous malignant melanoma," *J. Cutan. Pathol.* **37**(2), 256–268 (2010).
46. M. Seiji and N. Otaki, "Ultrastructural studies on Harding-Passey mouse melanoma," *J. Invest. Dermatol.* **56**(6), 430–435 (1971).
47. J. A. Hunter et al., "Cellular fine structure in the invasive nodules of different histogenetic types of malignant melanoma," *Br. J. Dermatol.* **98**(3), 255–272 (1978).
48. K. Wolff, "Melanocyte-keratinocyte interactions in vivo: the fate of melanosomes," *Yale J. Biol. Med.* **46**(5), 384–396 (1973).
49. K. Wolff and H. Honigsmann, "Are melanosome complexes lysosomes?" *J. Invest. Dermatol.* **59**(2), 170–176 (1972).
50. J. Borovansky et al., "Attempts to induce melanosome degradation in vivo," *Folia Biol. (Praha)* **45**(2), 47–52 (1999).
51. W. Korytowski and T. Sarna, "Bleaching of melanin pigments. Role of copper ions and hydrogen peroxide in autooxidation and photooxidation of synthetic dopa-melanin," *J. Biol. Chem.* **265**(21), 12410–12416 (1990).
52. A. E. Dontsov et al., "Effect of UV radiation and hydrogen peroxide on the antiradical and antioxidant activities of DOPA melanin and melanosomes from retinal pigment epithelial cells," *Russ. Chem. Bull.* **64**(7), 1623–1628 (2015).
53. C. H. Liu et al., "Melanin bleaching with dilute hydrogen peroxide: a simple and rapid method," *Appl. Immunohistochem. Mol. Morphol.* **21**(3), 275–279 (2013).
54. J. Borovansky and M. Elleder, "Melanosome degradation: fact or fiction," *Pigm. Cell Res.* **16**(3), 280–286 (2003).
55. M. Mastore, L. Kohler, and A. J. Nappi, "Production and utilization of hydrogen peroxide associated with melanogenesis and tyrosinase-mediated oxidations of DOPA and dopamine," *FEBS J.* **272**(10), 2407–2415 (2005).
56. M. Picardo et al., "Correlation between antioxidants and phototypes in melanocytes cultures. A possible link of physiologic and pathologic relevance," *J. Invest. Dermatol.* **113**(3), 424–425 (1999).
57. F. Liu-Smith, R. Dellinger, and F. L. Meyskens, "Updates of reactive oxygen species in melanoma etiology and progression," *Arch. Biochem. Biophys.* **563**, 51–55 (2014).
58. W. E. Carson, III, "ASCO 2015 update on melanoma," *Surg. Oncol.* **24**(4), 363–365 (2015).
59. K. Y. Ju et al., "Bioinspired polymerization of dopamine to generate melanin-like nanoparticles having an excellent free-radical-scavenging property," *Biomacromolecules* **12**, 625–632 (2011).
60. J. Pyo, K. Y. Ju, and J. K. Lee, "Artificial pheomelanin nanoparticles and their photo-sensitization properties," *J. Photochem. Photobiol. B* **160**, 330–335 (2016).

Kuk-Youn Ju received his PhD in chemistry from Seoul National University. His research focuses on establishment of structure-property-function relationship for natural pigment systems and their application as functional materials.

Simone Degan received his PhD from the faculty of Medicine at Cranfield Postgraduate Medical School, England, in 2005. He then joined the Department of Pathology at Duke University studying respiratory diseases in infants and adults. In 2010 he joined the Departments of Chemistry and Radiology, studying melanomas and lung cancer. He is now conducting research for the Departments of Chemistry, Radiology, Neurosurgery, Dermatology, and Cell Biology on a variety of preclinical model of diseases.

Martin Fischer received his PhD in physics from the University of Texas, Austin, in 2001. He then joined Bell Labs/Agere Systems, where he worked on high-speed optical fiber networks. In 2003 he moved to the University of Pennsylvania to perform research on laser microscopy in skin and gas MRI in lungs. In 2005 he moved to Duke University, where he is now exploring novel optical techniques for molecular three-dimensional imaging in highly complex materials.

Kevin C. Zhou received his BS degree in biomedical engineering from Yale University in 2015. Currently, he is a PhD student in the biomedical engineering department at Duke University, where his research focuses on technology development at the intersection of the fields of optical coherence tomography, pump-probe microscopy, and computational imaging.

Xiaomeng Jia received her BS degree at Shandong University. She is a PhD candidate in the Physics Department, Duke University. Her research focuses on exploring the properties of the nonlinear processes in pump-probe microscopy and using the knowledge to improve the imaging performance and data analysis.

Jin Yu received her PhD in chemistry from Duke University in 2018. Her research interest focuses on the investigation of photo-physical dynamics of various chemicals (e.g. artwork pigments, semiconducting materials, and melanin) using nonlinear optical microscopy.

Warren S. Warren is the James B. Duke Professor of Chemistry, Physics, Radiology and Biomedical Engineering at Duke University. He received his AB degree from Harvard in 1977 and his PhD from UC Berkeley in 1980. He did postdoctoral work with Ahmed Zewail at Caltech, moved to the Princeton faculty in 1982, and moved to Duke in 2005. His research focused on coherent spectroscopy (both magnetic resonance and optical).